

RSC Advances



This is an *Accepted Manuscript*, which has been through the Royal Society of Chemistry peer review process and has been accepted for publication.

Accepted Manuscripts are published online shortly after acceptance, before technical editing, formatting and proof reading. Using this free service, authors can make their results available to the community, in citable form, before we publish the edited article. This *Accepted Manuscript* will be replaced by the edited, formatted and paginated article as soon as this is available.

You can find more information about *Accepted Manuscripts* in the [Information for Authors](#).

Please note that technical editing may introduce minor changes to the text and/or graphics, which may alter content. The journal's standard [Terms & Conditions](#) and the [Ethical guidelines](#) still apply. In no event shall the Royal Society of Chemistry be held responsible for any errors or omissions in this *Accepted Manuscript* or any consequences arising from the use of any information it contains.



RSC Advances

COMMUNICATION

Hybrid organic-inorganic layered TiO₂ based nanocomposite for sunlight photocatalysis

Received 00th January 20xx,
Accepted 00th January 20xx

DOI: 10.1039/x0xx00000x

www.rsc.org/

Eglantina Benavente^{a,e}, Carlos Maldonado^{a,e}, Sindy Devis^{b,e}, Leslie Diaz^{c,e}, Harold Lozano^{b,e}, Clivia Sotomayor-Torres^d and Guillermo González^{b,e}.

A novel hybrid nanocomposite constituted of single TiO₂ nanosheets sandwiched between stearic acid self-assembled monolayers was synthesized and tested in the photodegradation of methylene blue under sunlight. The product showed better photocatalytic performance than anatase under similar conditions, which may be further improved through sensitization with cadmium sulfide.

Introduction

Wide-bandgap semiconductors such as TiO₂, ZnO, and SnO₂ have received much attention because of their promising applications in waste-water purification, as well as solar energy conversion.¹⁻⁴ Nanostructured TiO₂-based photocatalysts remain the most promising materials owing to their high photoactivity, physical and chemical stability, nontoxicity, and low cost.^{5,6} However, restrictions like the fast recombination of the photogenerated electron/hole (e⁻/h⁺) and poor harvesting of visible light limit the use of TiO₂ in cost-effective environmental remediation processes. Numerous approaches to solve the drawbacks of TiO₂ have been reported.^{7,8} Among them, the extension of TiO₂ absorption towards lower energies by creating electronic levels within its bandgap, for instance by doping TiO₂ with metal or non-metal species⁹⁻¹⁴ and, very recently, by coating the crystalline stoichiometric TiO₂ with a shell rich in defects of amorphous black TiO₂.^{15,16} TiO₂ sensitization with dyes or other semiconductors has been also widely used.^{6-8,17-19} Improved photocatalysts have been obtained by the coupling of

CdS with low-dimensional nanostructures of TiO₂ tubes, rods, wires or nanosheets,²⁰⁻²³ possibly due to a reduced photoinduced charge carrier recombination rate, promoted by the higher aspect ratio of the particles. The photocatalyst capability for adsorbing organic pollutants at its surface, though only rarely considered until now,²⁴ is also relevant for designing efficient catalysts.

This communication focuses on the photocatalytic behavior of a new organic-inorganic hybrid nanocomposite, TiO₂(stearic acid)_{1.1}x 0.6H₂O (LHTiO₂), where both the low dimensionality of TiO₂ and the adsorption ability of the organic component are conjugated. The photoactivity of this nanocomposite, both as-prepared and sensitized by CdS, was tested regarding the degradation of aqueous methylene blue (MB) under sunlight. The results were clearly improved with respect to that of anatase under similar conditions.

The LHTiO₂ nanocomposite was prepared by the reaction of titanium tetraisopropoxide (TTIP) with stearic acid in ethanol. The SEM images of the product (Fig. 1A and B) reveal microstructured aggregates of particles with a lamellar morphology. The XRD pattern of the product (Fig. 2A) corroborates the lamellar nature of the nanocomposite. The diffraction peaks at 2θ values of 2.98°, 6.10° and 9.17° are in good agreement with the three first (00l) reflections in a lamellar solid with a basal-distance along the c-axis of 29.6 Å. The low intensity peaks at 20.21° and 21.39° may be ascribed to a small excess of free stearic acid (JCPDS 03-0252). The average thickness of the nanosheets, 18 nm, was estimated by the Scherrer equation and approximately corresponds to six single sheets of the hybrid per particle.²⁵ The Raman spectrum of as-prepared LHTiO₂ (Fig. 2C), did indicate the product was defect-rich and poorly crystalline. Spite of that, the more prominent features in the spectrum could be assigned to several of the vibration modes reported for the TiO₂(B)²⁶ (arrows in Fig. 2C). In turn, the spectra of TiO₂ samples calcined at 185 y 500°C (Fig. S1[†]) showed that the TiO₂(B) phase was thermally instable. The spectrum of the sample calcined at 185°C corresponded to a completely amorphous material; no peak of any stable TiO₂ phases was apparent; and only some few features from residual carboxylic acid (Fig. S1[†]) were identifiable. At 500 °C the LHTiO₂ became quantitatively into pure anatase.

^a Universidad Tecnológica Metropolitana, P.O. Box 9845, Santiago, Chile. Tel: 56-227877109; E-mail: ebenaven@utem.cl

^b Universidad de Chile, P.O. Box 653, Santiago, Chile

^c Universidad de Santiago de Chile, P.O. Box 10233, Santiago, Chile

^d Catalan Institute of Nanotechnology (CIN2-CSIC) Campus Bellaterra, Spain

^e Center for the Development of Nanoscience and Nanotechnology, CEDENNA, Santiago, Chile

[†] Electronic Supplementary Information (ESI) available: [Experimental section and additional characterization]. See DOI: 10.1039/x0xx00000x

Both elemental and thermogravimetric analysis (Fig. S2†) of the product indicate the formation of a commensurate nanocomposite $\text{TiO}_2(\text{stearic acid})_x \cdot 0.6\text{H}_2\text{O}$ (LHTiO₂), with a ~10% excess of free carboxylic acid. Figs. 2B and 2C shows the UV-vis diffuse-reflectance spectra of samples of as-prepared LHTiO₂ and TiO₂ anatase. The photoresponse of LHTiO₂ in the UV region is qualitatively similar to that of anatase. However, the band-edge in the spectrum of the nanocomposite (insert in Fig. 2B) was slightly blue-shifted, with respect to that of TiO₂, corresponding to an increase in the bandgap of about 0.1 eV, which could be ascribed to 2D confinement of the semiconductor. In order to identify the role of carboxylic acid in the nanocomposite, we analyzed the infrared spectrum of the product (Fig. S3†). The two bands at 1560 and 1315 cm^{-1} , corresponding to the asymmetric and symmetric $\nu(\text{C-O})$ modes, respectively, demonstrate that the organic moiety is found as a carboxylate mono-coordinated to the inorganic sheets.²⁷ The low intensity $\nu(\text{C-O})$ band at 1705 cm^{-1} corroborates the presence of a small amount of free acid in the sample. According to the available evidence, the LHTiO₂ nanocomposite can be described as a two-phase nanostructure in which carboxylic acid is intercalated between inorganic sheets (Fig S4†).

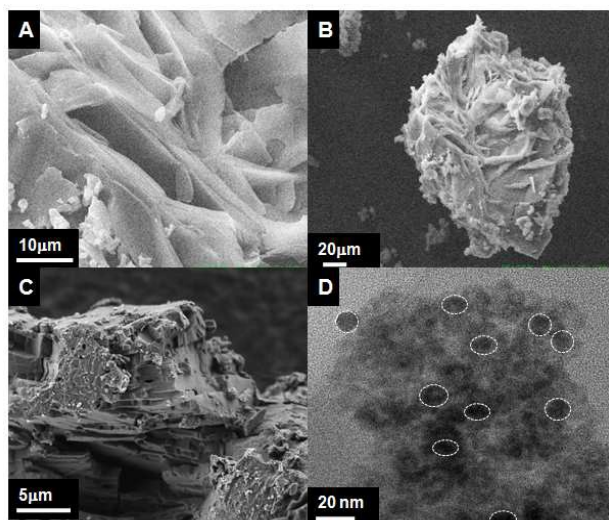


Fig. 1 SEM images of LHTiO₂ (A and B), SEM images of LHTiO₂/CdS0.05 (C) and TEM images of LHTiO₂/CdS0.05, CdS NPs featured in circles in the image (D).

The photocatalytic performance of LHTiO₂ was tested for the photodegradation of methylene blue (MB) under sunlight, in aqueous solution and ambient conditions. The photocatalytic efficiency of LHTiO₂ after 220 min irradiation, about 49%, was significantly higher than that of anatase under similar conditions, i.e. about 20% (Fig. 2D); this occurred in spite of the slightly larger band gap of LHTiO₂. The increased photoactivity of LHTiO₂ under visible light could be caused by the almost imperceptible extent of its absorption band (Fig. 2B and Fig. S5†). This effect appears to correspond to the Urbach tail which has been explained by the creation of discrete electronic levels inside the TiO₂ band gap (Fig. S6†).^{28,29}

To further investigate the photocatalytic behavior of LHTiO₂, CdS-sensitized LHTiO₂ was fabricated using cadmium sulfide nanoparticles (CdS NPs) (JCPDS 10-0454, Fig S7†). Four composite samples containing 0.1, 0.05, 0.025, and 0.0125 moles of CdS per mole of titanium oxide were prepared by mixing the components under sonication. SEM images (Fig. 1C) revealed that the lamellar nature of the precursor LHTiO₂ was retained in the composites. No changes were observed in DRX after adding CdS, probably due to the low concentration (<5%) of the latter. The TEM image of the LHTiO₂/CdS 1:0.05 sample showed CdS NPs ~10-18 nm in size, featured in circles in the image (Fig. 1D). The EDX spectrum (Fig. S8†) corroborated the presence of cadmium and sulfur in the sample. The UV-vis-diffuse reflectance spectra (Fig. 3A) showed that the absorption edge at 373 nm in the LHTiO₂ was extended to ~575 nm in the composite. The photocatalytic properties of as-prepared CdS/LHTiO₂ composites were evaluated under conditions similar to those used for LHTiO₂ (MB concentration, sunlight, room temperature). Among the tested samples, the one with 0.05 moles of CdS per mole of titanium showed the highest photocatalytic efficiency (Fig. S9†). The comparison of catalytic activity of this sample with those of its components LHTiO₂ and CdS NPs and with anatase (Fig. 3A) indicated that, after 220 min of sunlight irradiation, 20%, 49%, 67%, and 90% of MB was degraded when using anatase, LHTiO₂, CdS NPs, and the LHTiO₂/CdS composite, respectively. The apparent rate constants (k_{app} , min^{-1}) for LHTiO₂/CdS were about 5 and 6 times faster than for LHTiO₂ and anatase, respectively (Fig. 3B). These results qualitatively agree with multiple reports on the improved photocatalytic efficiency of nanostructured TiO₂ with the presence of CdS.¹⁹⁻²³

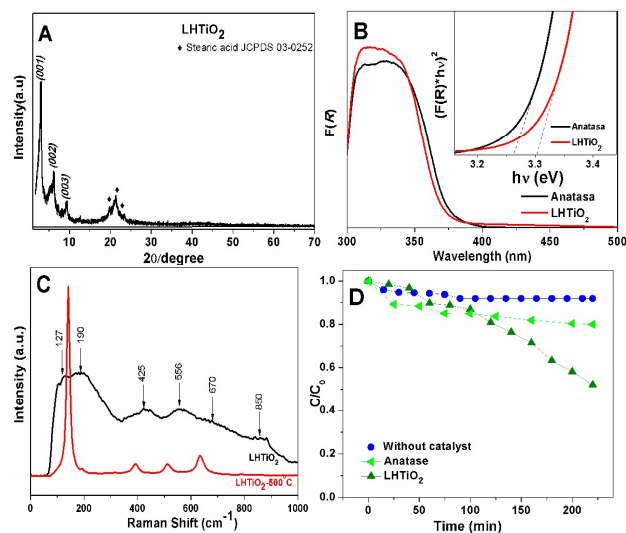


Fig. 2 XRD patterns of LHTiO₂ (A), UV-vis diffuse reflectance spectra of anatase and LHTiO₂, in insert, band gap are calculated according to Kubelka-Munk function (see supplementary information) (B), Spectra Raman of LHTiO₂ and LHTiO₂ calcined at 500°C (C) Plots of the degradation of MB solution under sunlight without catalyst, in the presence of LHTiO₂ and of anatase (D).

The photocatalytic performance of LHTiO₂ and LHTiO₂/Cd under sunlight could be to some extent correlated with their absorption in

the visible spectrum (Fig. 3A). However, the nature of these two phenomena is probably different. In the former, the creation of new electronic states could occur in the band gap of TiO₂, while in LHTiO₂/CdS, visible light absorption should preferably occur in CdS, due to its narrow band gap, i.e. through sensitization arising from the junction of both semiconductors. The shape of the MB spectrum recorded in the range 200-750nm remained practically unaltered throughout the process and the formation of any organic subproduct was not detected, thus pointing to the mineralization of the dye (Fig. S10[†]). The XRD pattern of LHTO₂/CdS after one photocatalysis cycle (Fig. S11[†]) indicated that the composite retained its lamellar nature but lost some crystallinity.

A probable mechanism for the degradation of MB over LHTiO₂/CdS is schematically illustrated in Fig. 3D. During irradiation, the photoinduced charge carriers are primarily created on the CdS nanoparticle. The photoexcited electron on the CdS conduction band (CB) can be easily transferred to the CB of the TiO₂ nanosheet owing to suitable matching between the energy positions of the conduction bands of both semiconductors, i.e. about 0.5 eV. Electrons accumulated on the inorganic moiety of LHTiO₂ can activate adsorbed molecular oxygen, producing superoxide radicals (O₂^{•-}). Further reduction of O₂^{•-} generates peroxide intermediates which decompose to hydroxyl radicals capable of accomplishing dye mineralization. The photogenerated holes stranded in the CdS cannot oxidize OH groups into hydroxyl radicals, but may instead oxidize the dye directly, or react with CdS itself (photocorrosion). However, the diminution in the photocatalytic efficiency of LHTiO₂/CdS with an excess of CdS (Fig. S9[†]), as well as the photocorrosion of the catalyst (Fig. S12[†]), indicates that the oxidation of MB by photo-holes is less important than that promoted by electrons on TiO₂.

To further understand the role of photogenerated radicals in MB degradation under sunlight, we carried out controlled experiments with the addition of either tert-butyl alcohol (TBA) or benzoquinone (BQ) as scavengers of hydroxyl radicals and O₂^{•-}, respectively.^{12,13,23} Only TBA slightly inhibited the photodegradation efficiency of LHTiO₂/CdS, corroborating a process mainly mediated by hydroxyl radicals. The low effect of the scavengers points to a protective effect of the organic surfactant, ensuring the oxidation process takes place at the TiO₂/carboxylic acid interface, far from the scavengers in the solution (Fig. S13[†]).

Conclusions

In summary, a new hybrid nanocomposite constituted of single TiO₂ nanosheets sandwiched between self-assembled long-chain carboxylic acid monolayers was prepared. The preliminary results show that this nanocomposite behaves as a semiconductor with photocatalytic activity in the degradation of methylene blue under sunlight with improved activity over anatase. This behaviour is attributed to the creation of new discrete electronic levels inside the TiO₂ bandgap. The photocatalytic performance of the product can be further enhanced through its sensitization with CdS. The catalytic behaviour of the as-prepared nanocomposite as well its successful sensitization with CdS can be attributed to the absorbent ability of its organic component.

Acknowledgments

The authors acknowledge the Universidad Tecnológica Metropolitana, Universidad de Chile, FONDECYT Grants 1151189 and 1131112, and CONICYT Grant FB0807 (CEDENNA). The authors would like to acknowledge Mr. Roberto Villarroel by Raman Spectroscopy measurements.

Notes and references

- H. J. Zhang, G. H. Chen, D. W. Bahnemann, *J. of Mater. Chem.*, 2009, **19**, 5089-5121.
- S. Hernández, D. Hidalgo, A. Sacco, A. Chiodoni, A. Lamberti, V. Cauda, E. Tresso, G. Saracco, *Phys. Chem. Chem. Phys.*, 2015, **17**, 7775-7786.
- L. Yang, Y. Jiao, Z. Zhang, F. Qu, A. Umar, X. Wu, *Appl. Mater. Interfaces*, 2014, **6**, 2174-2184.
- D. Deng, S. Martin, S. Ramanathan, *Nanoscale*, 2010, **2**, 2685-2691.
- R. Daghrir, P. Drogui, D. Robert, *Ind. Eng. Chem. Res.*, 2013, **52**, 3581-3599.
- S. G. Kumar, L.G. Devi, *J. Phys. Chem. A*, 2011, **114**, 13211-13241.
- N. Zhang, S. Liu, X. Fu, Y. Xu. *J. Phys. Chem. C*, 2011, **115**, 9136-9145.
- S. B. Rawal, S. Bera, D. Lee, D. Jang, W. In Lee, *Catal. Sci. Technol.*, 2013, **3**, 1822-1830.
- H. Xu, S. Ouyang, L. Liu, P. Reunchan, N. Umezawa, J. Ye, *J. Mater. Chem. A*, 2014, **2**, 12642-12661.
- S. Mazumdar, A. Bhattacharyya, *RSC Adv.*, 2015, **5**, 34942.
- C. Xue, T. Wang, G. Yang, B. Yang, S. Ding, *J. Mater. Chem A* 2014, **2**, 7674-7679.

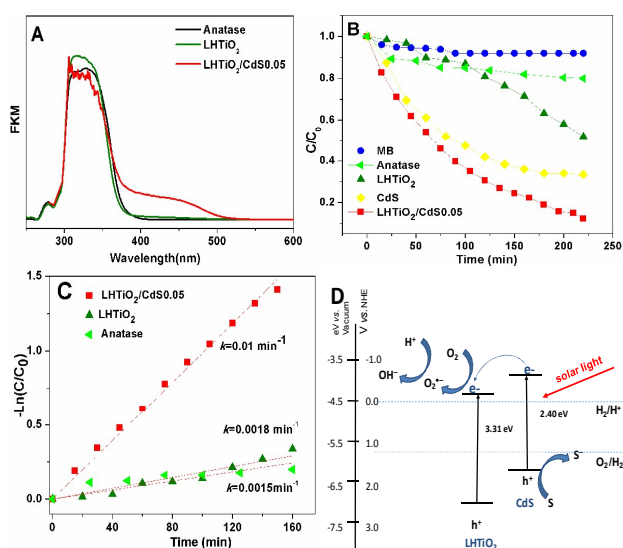


Fig. 3 UV-vis diffuse reflectance spectra of anatase, LHTiO₂ and LHTiO₂/CdS (A), Plots of the degradation of MB solution under sunlight of anatase, LHTiO₂, CdS NPs and LHTiO₂/CdS0.05 (B), Kinetic degradation of anatase, LHTiO₂ and LHTiO₂/CdS0.05(C), Schematic illustration the photocatalytic mechanism of LHTiO₂/CdS. (D)

- 12 J. Zhang, N. Zhang, Z. Tang, Y. Xu, *Chemical Science*, 2012, **3**, 2812-2822
- 13 S. Liu, N. Zhang, Z. Tang, Y. Xu, *Appl. Mater. Interfaces*, 2012, **4**, 6378-6385.
- 14 J. Luo, L. Ma, T. He, C. Ng, S. Wang, H. Sun, H. Fan, *J. Phys. Chem. C*, 2012, **116**, 11956-11963.
- 15 X.B. Chen, L. Liu, P.Y. Yu, S.S. Mao, *Science*, 2011, **331**, 746-750.
- 16 L. Xin, X. Liu, *RSC Adv.*, 2015, **5**, 71547-71550.
- 17 P. Chowdhury, J. Moreira, H. Gooma, A. K. Ray, *Ind. Eng. Chem. Res.* 2012, **51**, 4523-4532
- 18 L. Wu, J. C. Yu, X. Fu, *J. of Molecular Catalysis A: Chemical* 2006, **244**, 25-32.
- 19 Z. Chen, Y. Xu, *Appl Mater Interfaces*, 2013, **5**, 13353-13363.
- 20 D. Baker, P.V. Kamat, *Adv. Func. Mater.*, 2009, **19**, 805-811.
- 21 Y. Xie, G. Ali, S. Hwa Yoo, S. Oh Cho, *Appl. Mater. Interfaces*, 2010, **2**, 2910-2914.
- 22 N. Qin, Y. Liu, W. Wu, L. Shen, X. Chen, Z. Li, L. Wu, *Langmuir*, 2015, **31**, 1203-1209.
- 23 J. Zhang, F. Xiao, G. Xiao, B. Liu, *New J Chem.*, 2015, **39**, 279-286.
- 24 J. Zhao, T. Wu, K. Wu, K. Oikawa, H. Hidaka, N. Serpone, *Environ. Sci. Technol.*, 1998, **32**, 2394-200.
- 25 H. N. Kim, T. W. Kim, I. Y. Kim, S. J. Hwang, *Adv. Funct. Mater.*, 2011, **21**, 3111-3118.
- 26 J.R. Jokisaari, D. Bayerl, K. Zhang, L. Xie, Y. Nie, D. G. Schlom, E. Kioupakis, G. W. Graham, X. Pan, *Chem. Mater.*, 2015, **27**, 7896-7902
- 27 C.B. Mendive, D. W. Bahnemann, M. A. Blesa, *Catalysis Today* 2005, **101**, 237-244.
- 28 F. Urbach, *Phys. Rev.*, 1953, **92**, 1324
- 29 H. Yaghoubi, Z. Li, Y. Chen, H.T. Ngo, V. R. Bhethanabotla, B. Joseph, S. Ma, R. Schlaf, A. Takshi, *ACS Catal.*, 2015, **5**, 327-335.

